AIAA JOURNAL
Vol. 31, No. 12, December 1993

Multidomain Spectral Solutions of High-Speed Flows over Blunt Cones

David A. Kopriva*
Florida State University, Tallahassee, Florida 32306

A shock-fitted multidomain spectral collocation method is used to solve steady inviscid supersonic flows over two blunt, axisymmetric cones. The calculations are compared to a conical flow solution and to experimental data.

I. Introduction

THE spectral solution of the so-called "blunt-body" problem was first presented in 1984.[1] Like the typical finite difference solution,[2] this calculation used shock fitting and a time-dependent mapping. Subsequent papers[3,4] showed that, in comparison to second-order finite difference calculations, the spectral method is more accurate for the same number of grid points and less costly for the same accuracy.

In this paper, we apply to the blunt-body problem a shock-fitted version of the multidomain spectral method developed over the last five years.[5-8] The multidomain approach adds several practical advantages to the standard spectral method.[9] First, local resolution of steep, though continuous, features is possible. Also, geometric complexity can be more easily handled. The resulting subproblems are less stiff: they take less work and can use larger time steps than a single-domain method with the same number of grid points. Finally, because most of the flow over long bodies is supersonic, a convenient marching by subdomains is possible.[8]

As examples, we solve inviscid flows around two blunt cones. The first problem is that of supersonic flow over a long, hyperboloidal cone. That solution will be compared to the conical flow solution of an equivalent sharp-nosed cone. The second problem is the flow over a straight cone with a spherically blunted nose. For this geometry, experimental data is available[10] at several Mach numbers and we compare our solutions with this data.

The problems considered here have two significant features that would present difficulty to the standard spectral method. First, because we consider long bodies, the total number of grid points must be large. For the stability of an explicit time-marching procedure, the timestep is related to the square of the number of grid points in each direction. Thus, a single-domain calculation would be prohibitively expensive.

The second feature plagues even finite difference methods.[11] Because of the curvature of the shock near the nose, a narrow entropy layer forms along the body. This narrow layer would be difficult and expensive to resolve with a standard spectral method, even if combined with a mapping. We resolve the layer efficiently by a narrow set of subdomains along the body. We note that a zonal approach was suggested (Ref. 11) for the finite difference resolution of the difficulty.

II. Multidomain Spectral Method

A schematic of the geometry that we consider is shown in Fig. 1. The (x,y) coordinates denote the axial and radial coordinates, respectively. The body of revolution is defined by its radius, $y_b(x)$. Ahead of the body is the bow shock and supersonic freestream. Since the shock will be fitted, we compute the solution only in the region between the shock and the body. The freestream conditions upstream of the shock are specified as boundary conditions.

Flows over two bodies are considered here. The first body is that of a hyperboloidal cone with unit radius of curvature at the nose and the height of the cone in (x,y) coordinates is given by

$$y_b = \tan(\delta)\sqrt{(x + x_0)^2 - \alpha^2}$$

where $\alpha = 1/\tan^2(\delta)$, δ is the asymptotic angle of the cone, and $x_0 = \alpha + 1$. The second geometry (Fig. 2) corresponds to the experimental setup of Cleary.[10]

The transformation of the region between the shock and the body to computational coordinates is done in two steps: $(x,y,t) \leftrightarrow (r,s,t) \leftrightarrow (X,Y,T)$. The first mapping is to a coordinate system where s represents the distance along the body (with $s = 0$ at the nose), and r is the normal distance from the body. In (r,s) coordinates, we create multiple nonoverlapping subdomains, denoted G_k, which collectively cover the region between the shock and the body (see Fig. 1). Each subdomain is bounded by four curves. In r, these bounds are $r_{\min}(s,t,k)$ and $r_{\max}(s,t,k)$. Time-dependent subdomain boundary positions are included to allow the shock boundary to move with time. Each of these subdomains is mapped individually to the unit square, $(X,Y) \in [0,1] \times [0,1]$ by the transformation

$$X_k = \frac{r - r_{\min}(s,t,k)}{r_{\max}(s,t,k) - r_{\min}(s,t,k)} \tag{1a}$$

$$Y_k = \frac{s - s_{\min}(k)}{s_{\max}(k) - s_{\min}(k)} \tag{1b}$$

$$T = t \tag{1c}$$

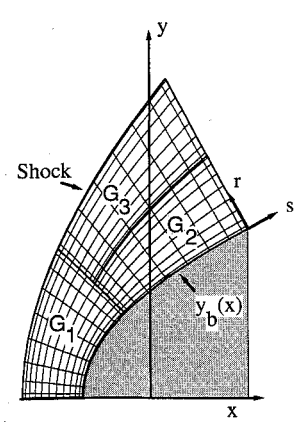

Fig. 1 Geometry of the blunt body problem.

Presented as Paper 92-0324 at the AIAA 30th Aerospace Sciences Meeting, Reno, NV, Jan. 6-9, 1992; received March 16, 1992; revision received March 15, 1993; accepted for publication April 5, 1993.

*Associate Professor, Department of Mathematics and Supercomputer Computations Research Institute. Member AIAA.

On each subdomain we solve the Euler gas-dynamics equations in the nonconservative form:

$$\begin{aligned} P_T + UP_X + VP_Y + \gamma[X_x u_X + X_y v_X + Y_x u_Y + Y_y v_Y + (v/y)] = 0 \\ u_T + Uu_X + Vu_Y + (a^2/\gamma)\,(X_x P_X + Y_x P_Y) = 0 \\ v_T + Uv_X + Vv_Y + (a^2/\gamma)\,(X_y P_X + Y_y P_Y) = 0 \\ S_T + US_X + VS_Y = 0 \end{aligned} \tag{2}$$

where $P = \ln(p)$ is the logarithm of the pressure, $q = (u,v)$ is the Cartesian velocity, and S is the entropy. The contravariant velocities are $U = X_t + uX_x + vX_y$ and $V = uY_x + vY_y$. The sound speed is defined by $a = \sqrt{\gamma}\,\exp\{[(\gamma - 1)P - S]/2\gamma\}$, where $\gamma = 1.4$. The quantities p, S, and the density ρ are scaled to the freestream values. Lengths are scaled to the nose radius. To justify the use of the nonconservation form, and to ensure that the spectral approximation is not used to approximate derivatives across the shock, the shock is fitted as a boundary.[3,4]

Within each subdomain, the spatial derivatives in the equations are approximated by a standard Chebyshev spectral collocation method.[9] The result of the approximation is a system of ordinary differential equations for the unknowns at each grid point. The system is advanced in time by a four-stage Runge-Kutta method.[9] Numerical experiments show that it is stable for a Courant number of at least three based on the smallest grid spacing.

The essential feature of the multidomain spectral method is the treatment of the interfaces between subdomains.[6,7] The treatment that we use allows for local refinement of the grid. Subdomains can be of any size and the number of grid points in each is independent of the number of grid points in its neighbors.

Interface conditions between subdomains for various types of interface points are described in detail in Refs. 7 and 8. We summarize the procedure here. The Eqs. (1) are solved on each subdomain to get the interior point solutions and (provisional) values of the flow quantities on the boundaries. Each interface point has at least two such provisional quantities, one from each subdomain to which it is a neighbor. These provisional quantities are then projected onto inflow and outflow components as follows. Four generalized Riemann variables are computed from the infinite number represented by $R = P + (\gamma/a)q \cdot \xi$, where ξ is a unit vector. The four choices are $\xi = \pm N$ and $\xi = \pm \tau$, where N and τ represent the normal and tangent vectors to the interface. To obtain the correct domain of dependence, the Riemann variables are then selected according to the subdomain from which their associated bicharacteristic comes. If the grid points do not match across the interface, the incoming quantities are interpolated using the natural Chebyshev interpolation that defines the method. The resulting Riemann variables are then recombined to get corrected values of the flow quantities.

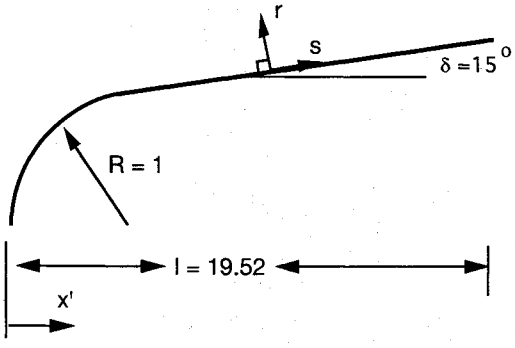

Fig. 2 Geometry of the blunt cone problem corresponding to the experiment of Ref. 10.

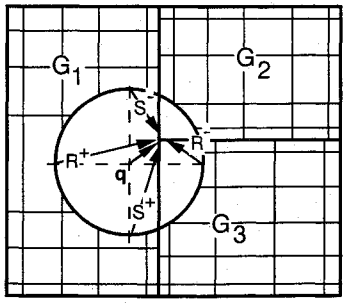

Fig. 3 Domain of dependence at the interface point between G_1, G_2, and G_3.

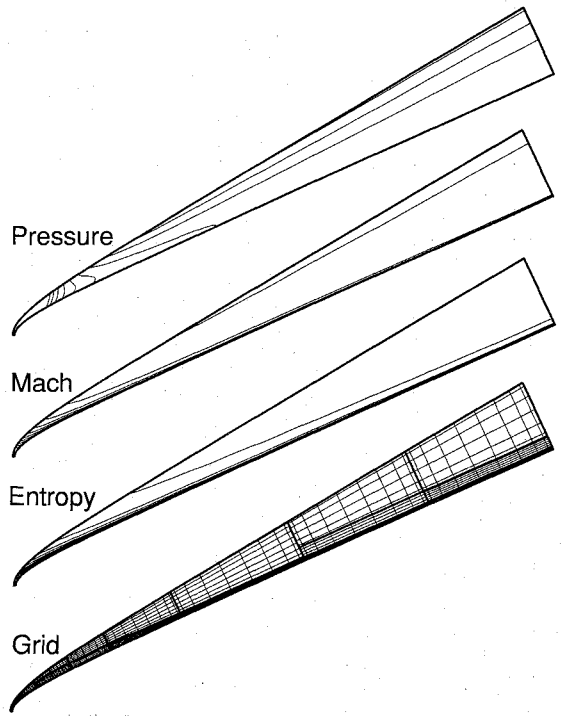

Fig. 4 Pressure, Mach number, and entropy contours with the computational grid for the Mach 4 flow over a 25-deg hyperboloidal cone.

As an example, we consider the computation of the flow quantities at the intersection point between the three domains G_1, G_2, and G_3 shown in Fig. 1. A schematic of this situation is shown in Fig. 3. In Ref. 7, this was called a "T" intersection. The difference now is that, because the top boundary is a moving boundary, the interfaces between G_1 and G_3 and between G_1 and G_2 move relative to each other. Superimposed on the grid of Fig. 3, we show a projection of the bicharacteristic cone that affects the interface point. We represent the base of the bicharacteristic cone by the circle. Since the length of the fluid velocity vector q is shown smaller than the sound speed represented by the radius of the circle, Fig. 3 shows a subsonic situation. Four bicharacteristics have been chosen corresponding to $\xi = \pm\hat{x}$, $\pm\hat{y}$. According to this choice, $R^+ = \tilde{P} + \gamma\,\tilde{u}/a$ and $S^\pm = \tilde{P} \pm \gamma\,\tilde{v}/a$ are computed from the provisional values $\tilde{P}$, $\tilde{u}$, and $\tilde{v}$ interpolated to the point in subdomain G_1, and the sound speed evaluated at the previous time level. R^- is computed from the interface point in G_3.

The interface condition requires that the true Riemann variables at the interface equal those computed from the provisional quantities.[7] Thus, we have four equations

$$\begin{aligned} P + (\gamma/a)\,u &= R^+ \\ P - (\gamma/a)\,u &= R^- \\ P + (\gamma/a)\,v &= S^+ \\ P - (\gamma/a)\,v &= S^- \end{aligned}$$

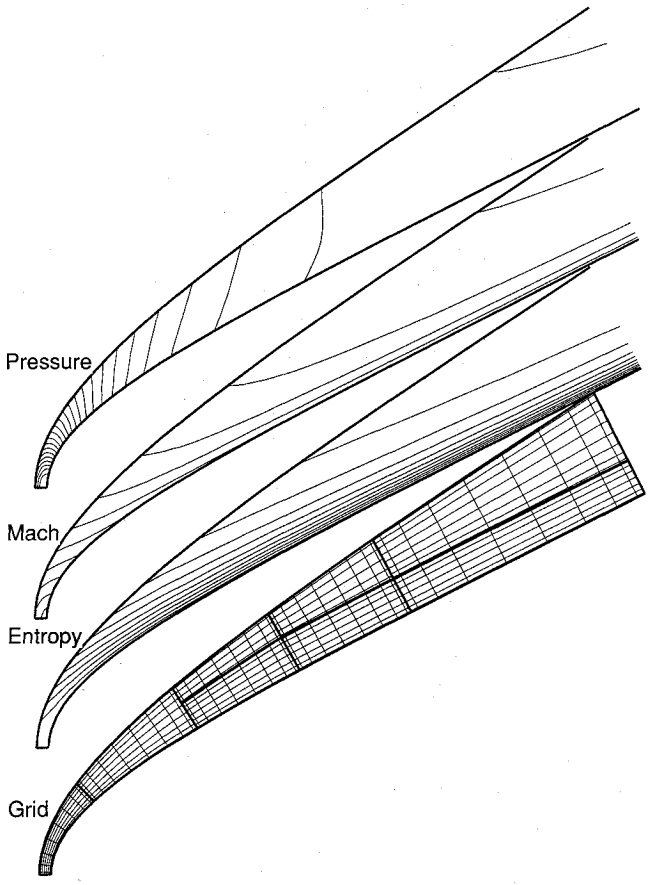

Fig. 5 Blowup of Fig. 4 in the region of the nose.

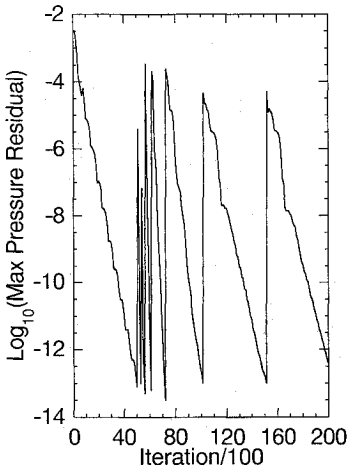

Fig. 6 Convergence of the pressure for the solution of Fig. 4. The jumps are the result of the marching by zones described in the text.

from which to calculate the three quantities, P, u, and v. Our choice of the four bicharacteristics makes the calculation of the velocities simple:

$$u = (a/2\gamma)\,(R^+ - R^-)$$

$$v = (a/2\gamma)\,(S^+ - S^-)$$

The pressure is computed by combining all four Riemann variables and subtracting the value computed in the upstream subdomain G_3 (see Ref. 7 for details).

$$P = \tfrac{1}{2}\,(R^+ + R^- + S^+ + S^- - 2\tilde{P}_1)$$

Finally, the entropy is advected along streamlines so its domain of dependence is given by the vector q shown in Fig. 3. Thus, the corrected value of the entropy is just the value computed in G_1, i.e., $S = \tilde{S}_1$. There is no essential complication in the fact that the interfaces move relative to each other, if necessary. We call such an interface a "shear interface." It is necessary only to update the grid connections and calculate the interpolation parameters at each timestep.

In fully supersonic flow, the interface procedure reduces to the conditions expected. At the outflow boundary, all Riemann variables are computed from the interior, so no external boundary condition is applied. At an inflow boundary, all Riemann variables are computed from the upstream subdomain so all variables are specified.

III. Results

Hyperboloidal Cone Problem

The first problem that we consider is the Mach 4 flow over a 25-deg hyperboloidal cone of length 50 nose radii. The solution contours and grid are shown in Fig. 4. A blowup of the region around the nose is shown in Fig. 5. As is typical for spectral multidomain calculations,[6,7] the solutions are smooth through the interfaces between subdomains, which are drawn on the grid plots as heavy lines. Clearly visible is the narrow entropy layer that forms along the body. To resolve this layer, we use a narrow strip of subdomains along the body. Outside the entropy layer, where the solution is nearly constant, a coarser grid is used.

The steady-state solutions of this and the problems in the next section were obtained by the zonal marching technique described in Ref. 8. A zone is a group of subdomains that have the same values of s_{min} and s_{max}. The solution on a subdomain containing only supersonic flow does not need to be computed until the subdomains upstream of it are converged. Subdomains downstream do not need to be computed until it is converged. Thus, only a fraction of the total grid needs to be solved at any given time, and the locally computed timestep can be used. Since the flow is supersonic over most of flowfield, this leads to an efficient solution technique for long bodies. Figure 6 shows the pressure residual history for the calculation in Figs. 4 and 5 for a residual tolerance set to 10^{-13}. As a zone converges, an initial condition extrapolated into the next zone and the calculation proceeds. For the convergence tolerance set to 10^{-5}, the calculation requires only 3400 timesteps and a total of 250 s on an IBM RS/6000 320H, which runs at approximately 4–5 mflops.

We can compare the solution of the flow over the hyperbolic cone to the conical flow solution over an equivalent sharp-nosed cone. As a test of the shock-fitting algorithm, Fig. 7 compares the shock shapes. First, far down the length of the cone, the shapes of both the body and the shock approach those of a sharp-nosed cone as required.

Outside the entropy layer, the flow between the shock and the body asymptotically approaches the conical result. Figure 8a–8c shows the pressure, velocity, and entropy at the exit

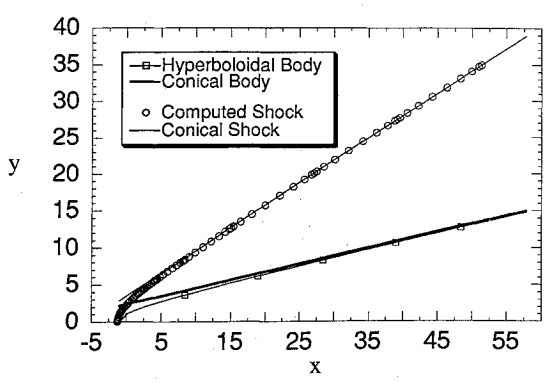

Fig. 7 Approach of the hyperboloidal cone and its computed shock to the sharp-nosed cone and its shock.

plane of the calculation shown in Fig. 4. The steep layer in the velocity and entropy is well resolved by the narrow subdomains near the body. Outside the entropy layer, the computed and expected results are indistinguishable. The pressure only appears to have the worst error of the three curves, but the effect is due to the scale. At the body, the error is only 0.09%. Finally, the shock wave occurs at the proper distance from the body.

Blunt Cone Problem

We have also solved the flow over the geometry shown in Fig. 2. This geometry corresponds to the $\delta = 15$ deg experi-

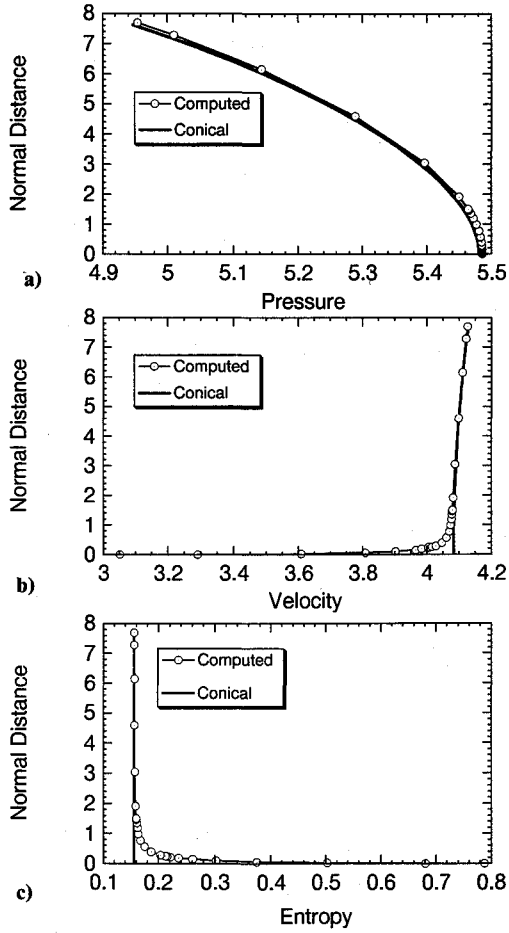

Fig. 8 Profiles of the computed pressure, velocity, and entropy at the exit plane of Fig. 4 compared to the conical flow solution.

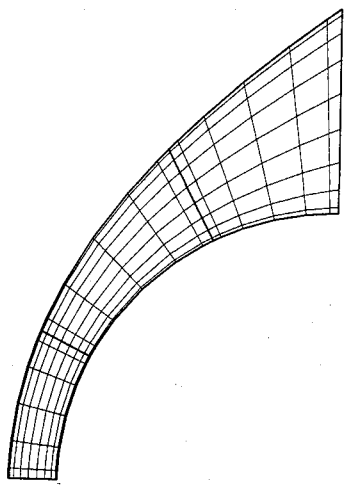

Fig. 9 Grid used to compute the spherical nose flows.

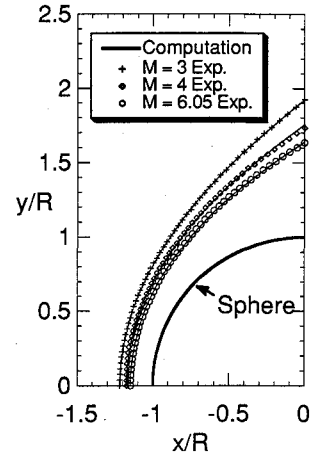

Fig. 10 Comparison of computed and experimental shock positions for supersonic flow over a sphere.

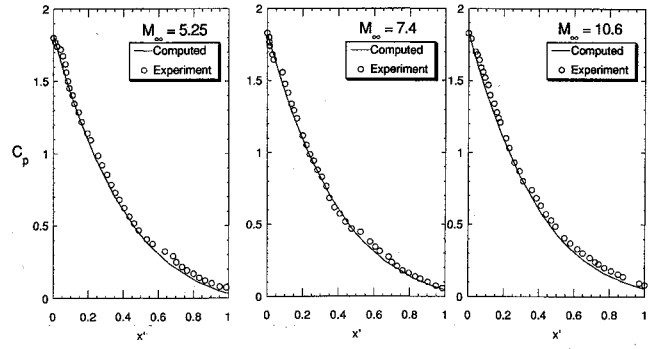

Fig. 11 Comparison of pressure coefficients on a spherical body.

ments of Cleary.[10] Freestream Mach numbers for his experiments were $M_\infty = 5.25$, 7.4, and 10.6. Experimental data were not obtained in the viscous boundary layer itself. Thus, Cleary claims that his data reflect an essentially inviscid flow, at least near the nose. We will compare computed solutions and the experimental results at all three Mach numbers. Data exists for two cones with half-angle $\delta = 15$ and 30 deg. Only the 15-deg cone will be considered, since the experimental data for this case shows far less scatter.

We begin our discussion of the results by considering the flow over the spherical nose only. For this problem, experimental measurements of shock positions were presented by Ryabinkov.[12] Measured pressure coefficients along the surface are presented by Cleary.[10]

Figure 9 shows the grid used to compute the flow over the spherical nose. In these calculations, three subdomains were used. As another test of the shock-fitting algorithm, Fig. 10 shows the computed shock positions and the experimental results of Ref. 12 for three freestream Mach numbers. Of the three cases, the computed standoff distances at the nose differ by at most 1.4%.

Figure 11 shows the computed and experimental pressure coefficients

$$C_p = (P_{\text{body}} - P_\infty)/(\gamma/2)\, p_\infty M_\infty^2$$

for the three Mach numbers in Cleary's experiments. In all three cases, the agreement is excellent, at least to within the scatter in the experimental data. Because of the way that the experiments were done, Cleary claims that the data should only be accurate to $x' = 0.75$. We still see good agreement for the larger values of x'.

We consider next the solution of the blunt cone problem itself. Figure 12 shows the contours of the pressure, Mach number, entropy, and the grid on which they were computed for the $M = 10.6$ case. Clearly visible in the pressure plot is the steep expansion wave generated at the joint between the cone

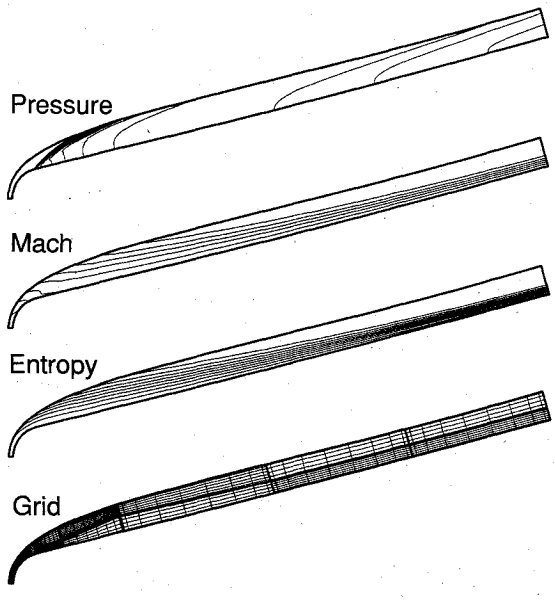

Fig. 12 Solution contours and grid for Mach 10 flow over a 15-deg blunt cone.

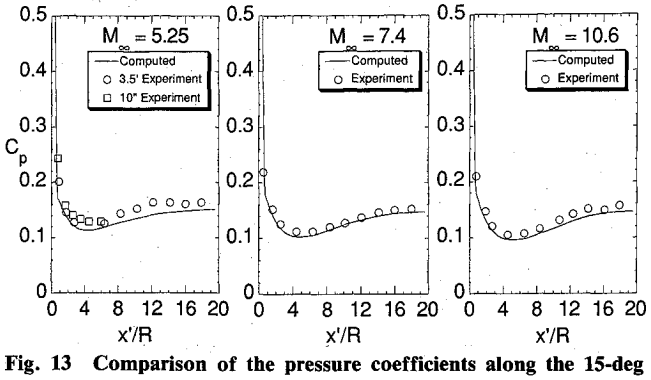

Fig. 13 Comparison of the pressure coefficients along the 15-deg cone.

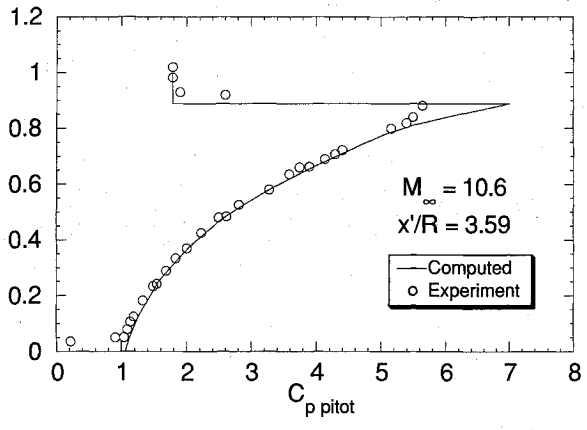

Fig. 14 Total pressure coefficient variation normal to the cone at $x' = 3.59$.

and the nose. Also apparent is the entropy layer that forms far downstream along the body. The subdomain decomposition and the distribution of grid points were chosen to resolve these features.

A comparison of the pressure coefficients along the cone surface is shown in Fig. 13. Here, again, we see good agreement, although the computation slightly underpredicts the experimental values. Agreement is better at the higher Mach numbers.

Experimental data for the variation of the solution normal to the cone surface is available at two stations, $x' = 3.59$ and $x' = 16.67$ for $M = 10.6$. The latter position shows viscous effects so we do not consider it here. The experimental data is given in terms of the pressure coefficient derived from the pitot pressure. We scale our results to match the pressure coefficient in the freestream.

Figure 14 shows the variation of the pitot pressure coefficient normal to the body at $x' = 3.59$. Recall that the nose ends at $x' = 1$. Thus $x' = 3.59$ represents a distance of three and one-half nose radii or 18% down the total length of the body. Since the shock is fitted, the solution upstream is known exactly, i.e., $p = \rho = 1$, $M = M_\infty$, and $S = 0$. The solution drawn on Fig. 14 beyond the shock represents that exact solution. Except at the shock and at the body, the computed solution represents the experimental data within the scatter of the data. Note also that although the true shock shows the effects of viscosity and the shock-fitted solution does not, the shock does occur in the correct place.

IV. Summary

A multidomain spectral code was developed to compute the steady inviscid axisymmetric flow over conical bodies. The calculations presented here include flows over a long (50 nose radii) 25-deg hyperbolic cone and over a 15-deg blunt-nosed straight cone. Other calculations of the flow over a hyperboloid involved cone half-angles between 10 and 30 deg and lengths up to 225 nose radii. The hyperboloidal cone solutions were compared to a conical flow. For the straight cone with a spherical nose, solutions at Mach numbers between five and 11 were compared to experiments.

Acknowledgments

The author would like to thank C. L. Streett and T. A. Zang for helpful discussions. This research was supported in part by the National Aeronautics and Space Administration under Grant NAG1-862 and by the U.S. Department of Energy through Contract DE-FC05-85ER250000.

References

[1]Hussaini, M. Y., Salas, M. D., and Zang, T. A., "Spectral Methods for Inviscid, Compressible Flows," *Advances in Computational Transonics*, edited by W. G. Habashi, Pineridge Press, Swansea, Wales, UK, 1984, pp. 875-912.

[2]Moretti, G., and Abbett, M., "A Time-Dependent Method for Blunt Body Flows," *AIAA Journal*, Vol. 4, 1966, pp. 2136-2141.

[3]Hussaini, M. Y., Kopriva, D. A., Salas, M. D., and Zang, T. A., "Spectral Methods for the Euler Equations: Part II—Chebyshev Methods and Shock-fitting," *AIAA Journal*, Vol. 23, No. 2, 1985, pp. 234-240.

[4]Kopriva, D. A., Zang, T. A., and Hussaini, M. Y., "Spectral Methods for the Euler Equations: The Blunt Body Problem Revisited," *AIAA Journal*, Vol. 29, No. 9, 1991, pp. 1458-1462.

[5]Kopriva, D. A., "A Spectral Multidomain Method for the Solution of Hyperbolic Systems," *Applied Numerical Mathematics*, Vol. 29, No. 9, 1986, pp. 221-241.

[6]Kopriva, D. A., "Solution of Hyperbolic Equations on Complicated Domains with Patched and Overset Chebyshev Grids," *SIAM Journal on Scientific and Statistical Computing*, Vol. 10, No. 1, 1989, pp. 120-132.

[7]Kopriva, D. A., "Multidomain Spectral Solution of the Euler Gas-Dynamics Equations," *Journal of Computational Physics*, Vol. 96, No. 2, 1991, pp. 428-450.

[8]Kopriva, D. A., "Spectral Solution of Inviscid Supersonic Flows Over Wedges and Axisymmetric Cones," *Computers and Fluids*, Vol. 21, No. 2, 1992, pp. 247-266.

[9]Canuto, C., Hussaini, M. Y., Quarteroni, A., and Zang, T. A., *Spectral Methods in Fluid Mechanics*, Springer-Verlag, New York, 1987, Chap. 8.

[10]Cleary, J. W., "An Experimental and Theoretical Investigation of the Pressure Distribution and Flowfields of Blunted Cones at Hypersonic Mach Numbers," NASA TN D-2969, 1965.

[11]Moretti, G., and Pandolfi, M., "Entropy Layers," *Computers and Fluids*, Vol. 1, No. 1, 1973, pp. 19-35.

[12]Ryabinkov, G. M., "Experimental Investigation of Flow Around Solids of Revolution in a Supersonic Gas Flow," *Supersonic Gas Flow Around Blunt Bodies*, edited by O. M. Belotserkowsky, NASA TT F-453, 1967, pp. 255-316.